Synthesis of Mesoporous Magnesium Oxide by CMK-3 Carbon Structure Replication

Jan Roggenbuck, Günter Koch, and Michael Tiemann*

Institut für Anorganische und Analytische Chemie, Justus-Liebig-Universität, Heinrich-Buff-Ring 58, D-35392 Giessen, Germany

Received March 29, 2006. Revised Manuscript Received June 14, 2006

Periodically ordered mesoporous magnesium oxide was synthesized in a double replication procedure. Mesoporous SBA-15 silica and CMK-3 carbon were successively used as hard structure matrixes. The carbon pore system was infiltrated with $Mg(NO_3)_2$, which was then converted to MgO at 573 K; the carbon matrix was finally removed by thermal combustion. The structure of the mesoporous MgO corresponds to that of the original SBA-15 silica. The products consist of hexagonally arranged cylindrical mesopores and crystalline pore walls. The efficiency of the replication series was studied by variation of the infiltration method and comprehensive pore size analysis of all involved mesoporous materials. The in situ formation of MgO inside the CMK-3 carbon pore system was monitored by thermal analysis. Postsynthetic treatment of the products at 823 K in a vacuum prior to removal of the carbon matrix was found to improve the crystallinity but to diminish the periodic order of the pore system.

Introduction

The utilization of self-assembled supramolecular aggregates of amphiphiles as structure-directing species is a well-established method for the synthesis of mesoporous materials with periodic and uniform pore systems.[1,2] However, this approach cannot be considered as a universal concept, since it is successful only for a limited variety of systems,[3] mainly for silica and aluminosilicate materials, which readily form amorphous phases. In many other systems, such as most metal oxides, the tendency to form dense, crystalline phases often leads to a phase separation of the amphiphilic species from the inorganic component during the formation of the solid. In other cases the inorganic network loses its nanoscopic periodic structure during the subsequent removal of the structure director, owing to insufficient condensation of the inorganic building units under the relatively mild thermal synthesis conditions. More recently, the concept of utilizing porous solids as rigid structure matrixes has extended the opportunities to create new ordered mesoporous materials.[4−6] The underlying concept of this approach is the creation of a negative replica of the structure matrix by infiltration of the pores with the respective precursor(s), in situ formation of the new solid material, and, finally, removal of the structure matrix. Contrary to supramolecular structure directors, such hard matrixes exclude the risk of phase separation while allowing for much higher synthesis temperatures, suitable for the generation of crystallinity within the pore walls. Mesoporous silica phases have served as replication matrixes for several mesoporous metal oxides, such as In_2O_3,[7] Co_3O_4,[8−12] Cr_2O_3,[8,13] WO_3,[14] Mn_xO_y,[8,10,15] CeO_2,[16] NiO,[8] Fe_2O_3,[8,17] and SnO_2.[10] Further opportunities arise from the utilization of mesoporous CMK-type carbon phases as structure matrixes. These are themselves synthesized by replication using mesoporous silica materials as matrixes.[18] The resulting mesoporous metal oxide is thus prepared by double replication; it is the negative replica of the parent carbon phase and the positive replica of the original silica phase. A major advantage of carbon matrixes is their facile and selective removal by thermal combustion in the final step of the replication. The removal of silica, by comparison, requires treatment with HF or concentrated NaOH, a procedure which often leads to the dissolution or structural disaggregation of the entire material. CMK-type carbon phases have been used as

* To whom correspondence should be addressed. E-mail: michael.tiemann@anorg.chemie.uni-giessen.de.

(1) Beck, J. S.; Vartuli, J. C.; Roth, W. J., Leonowicz, M. E.; Kresge, C. T.; Schmitt, K. D.; Chu, C. T.-W.; Olson, D. H.; Sheppard, E. W.; McCullen, S. B.; Higgins, J. B.; Schlenker, J. L. *J. Am. Chem. Soc.* **1992**, *114*, 10834−10843.
(2) Zhao, D.; Huo, Q.; Feng, J.; Chmelka, B. F.; Stucky, G. D. *J. Am. Chem. Soc.* **1998**, *120*, 6024−6036.
(3) Schüth, F. *Chem. Mater.* **2001**, *13*, 3184−3195.
(4) Schüth, F. *Angew. Chem., Int. Ed.* **2003**, *42*, 3604−3622.
(5) Yang, H.; Zhao, D. *J. Mater. Chem.* **2005**, *15*, 1217−1231.
(6) Lu, A.-H.; Schüth, F. *C. R. Chimie* **2005**, *8*, 609−620.
(7) Yang, H.; Shi, Q.; Tian, B.; Lu, Q.; Gao, F.; Xie, S.; Fan, J.; Yu, C.; Tu, B.; Zhao, D. *J. Am. Chem. Soc.* **2003**, *125*, 4724−4725.
(8) Tian, B.; Liu, X.; Yang, H.; Xie, S.; Yu, C.; Tu, B.; Zhao, D. *Adv. Mater.* **2003**, *15*, 1370−1374.
(9) Smått, J.-H.; Spliethoff, B.; Rosenholm, J. B.; Lindén, M. *Chem. Commun.* **2004**, 2188−2189.
(10) Smått, J.-H.; Weidenthaler, C.; Rosenholm, J. B.; Lindén, M. *Chem. Mater.* **2006**, *18*, 1443−1450
(11) Wang, Y.; Yang, C.-M.; Schmidt, W.; Spliethoff, B.; Bill, E.; Schüth, F. *Adv. Mater.* **2005**, *17*, 53−56.
(12) Jiao, F.; Shaju, K. M.; Bruce, P. G. *Angew. Chem., Int. Ed.* **2005**, *44*, 6550−6553.
(13) Zhu, K.; Yue, B.; Zhou, W.; He, H. *Chem. Commun.* **2003**, 98−99.
(14) Zhu, K.; He, H.; Xie, S.; Zhang, X.; Zhou, W.; Jin, S.; Yue, B. *Chem. Phys. Lett.* **2003**, *377*, 317−321.
(15) Imperor-Clerc, M.; Bazin, D.; Appay, M.-D.; Beaunier, P.; Davidson, A. *Chem. Mater.* **2004**, *16*, 1813−1821.
(16) Laha, S. C.; Ryoo, R. *Chem. Commun.* **2003**, 2138−2139.
(17) Jiao, F.; Harrison, A.; Jumas, J.-C.; Chadwick, A. V.; Kockelmann, W.; Bruce, P. G. *J. Am. Chem. Soc.* **2006**, *128*, 5468−5474.
(18) Ryoo, R.; Joo, S. H.; Jun, S. *J. Phys. Chem. B* **1999**, *103*, 7743−7746.

10.1021/cm060740s CCC: $33.50
Published on Web 07/20/2006

replication matrixes for mesoporous SiO_2[19,20] as well as for some mesoporous metal oxides, notably Al_2O_3, ZrO_2, and TiO_2.[21] We have recently tentatively presented the first synthesis of periodically ordered mesoporous MgO by utilization of CMK-3 carbon as the structure matrix.[22] Formerly, activated carbons[23] as well as carbon aerogels[24] have served as matrixes for porous MgO with nonuniform pore systems and broad pore size distributions. Here we present a detailed report on the synthesis of ordered mesoporous MgO, including the extension of the formerly reported results to products with crystalline pore walls as well as a comprehensive study on the impact of various synthesis parameters.

Experimental Section

SBA-15 silica was synthesized in a modification of a literature procedure.[2] A 12.0 g sample of P-123 block copolymer (Sigma) was mixed with 360 g of water and 43.0 g of HCl (32%). After addition of 24.0 g of tetraethyl orthosilicate (TEOS; Merck) the mixture was stirred at 308 K for 24 h. The resulting gel was transferred to a Teflon-lined autoclave and kept at 413 K for 24 h. The solid product was filtered off, washed with water, and calcined at 823 K for 6 h (heating rate 2 K min^{-1}). CMK-3 carbon was prepared according to a literature procedure.[25] The following wet impregnation procedure was used for the synthesis of mesoporous MgO, unless otherwise noted: A 1 g sample of CMK-3 was dispersed in 20 mL of an aqueous solution (1.0 mol L^{-1}) of $Mg(NO_3)_2$ (Merck) and the resulting solution stirred for 2 h to impregnate the carbon mesopores with $Mg(NO_3)_2$. After filtration and drying, the sample was heated under an air atmosphere to 573 K at a constant rate of 2.5 K min^{-1}, to convert magnesium nitrate to magnesium oxide. This procedure was repeated once. Crystalline products were obtained by keeping the sample at 573 K for 3 h. The carbon was removed by heating the sample under an air atmosphere to 1023 K at a constant rate of 2.5 K min^{-1} and keeping the sample at that temperature for 2 h.

Powder X-ray diffraction was carried out on a Bruker AXS D8 Advance diffractometer equipped with a secondary monochromator and automatic divergence slits (filtered Cu Kα radiation, 40 kV, 40 mA); the counting time was 2 s in steps of $2\theta = 0.01°$ for low-angle measurements ($2\theta < 10°$) and 8 s in steps of $2\theta = 0.02°$ for wide-angle measurements ($2\theta > 10°$). Nitrogen physisorption was conducted at 77 K on a Quantachrome Autosorb 6; samples were degassed at 393 K for 24 h prior to measurement. For data processing the Quantachrome Autosorb software comprising the NLDFT kernels "N_2 silica at 77 K, cylindrical pore model" and "N_2 carbon at 77 K, slit-pore model" was used. Transmission electron microscopy (TEM) and selected-area electron diffraction (SAED) were performed on a Philips CM30-ST microscope; for energy-dispersive X-ray (EDX) analysis an EDAX PV 9900 was used. IR spectroscopy was conducted on a Bruker FS25 spectrometer. Thermal analysis (thermogravimetry (TG)/mass spectrometry (MS)) was carried out under O_2/argon (20/80) flow with a Netzsch STA409PC thermobalance coupled with a Balzers QMG421 quadrupole mass spectrometer.

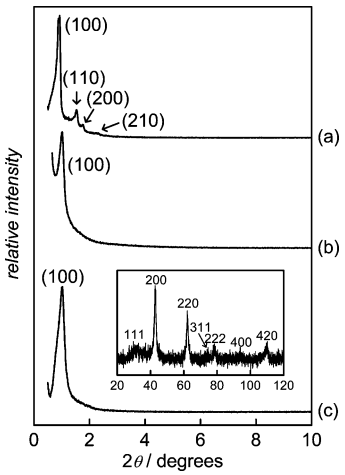

Figure 1. Powder X-ray diffraction diagrams of (a) SBA-15 silica, (b) CMK-3 carbon, and (c) mesoporous MgO. The low-angle reflections correspond to the hexagonal (*p6mm*) arrangement of the pores (indices in parentheses). The inset shows wide-angle reflections assignable to crystalline MgO (rock salt structure, indices without parenthesis).

Results and Discussion

Figure 1 shows the powder X-ray diffraction diagram of mesoporous MgO; the preceding SBA-15 silica and CMK-3 carbon phases which consecutively served as the structure matrixes are shown in the same graph. Low-angle reflections, corresponding to the two-dimensional hexagonal periodicity of the pore systems, are visible in all three samples. The resultant MgO material can be considered as the positive replica of SBA-15 silica (and as the negative replica of CMK-3 carbon), although a certain degree of broadening and a poorer resolution of the reflections indicate some loss in structural order. In the low-angle diffraction diagrams of CMK-3 and MgO only the 100 reflection can be identified; other low-angle reflections are not resolved and are only weakly visible as broad shoulders. The first replication step (SBA-15 to CMK-3) entails a slight shrinkage of the periodic distance, indicated by a shift of the reflections toward wider diffraction angles; this is frequently observed in this kind of silica-to-carbon replication.[25] However, no significant further change in the reflection angles is observed in the second replication step (CMK-3 to MgO); the d_{100} values of all three samples are listed in Table 1.

The wide-angle powder X-ray diffraction diagram of mesoporous MgO (Figure 1, inset) exhibits reflections attributable to the crystalline (rock salt) structure of magnesium oxide; such crystallinity is observed when the sample is kept at 573 K for 3 h after conversion of $Mg(NO_3)_2$ to MgO within the carbon matrix. To confirm that the crystallinity exists in the mesoporous samples rather than in potential nonporous byproducts, TEM was combined with SAED. Figure 2 shows a representative TEM image together with the SAED pattern from the same part of the sample. The TEM image is representative of the entire sample, showing long-range periodicity in the hexagonal pore arrangement. No indication of sub-

(19) Lu, A.-H.; Schmidt, W.; Taguchi, A.; Spliethoff, B.; Tesche, B.; Schüth, F. *Angew. Chem., Int. Ed.* **2002**, *41*, 3489−3492.
(20) Kang, M.; Yi, S. H.; Lee, H. I.; Yie, J. E.; Kim, J. M. *Chem. Commun.* **2002**, 1944−1945.
(21) Dong, A.; Ren, N.; Tang, Y.; Wang, Y.; Zhang, Y.; Hua, W.; Gao, Z. *J. Am. Chem. Soc.* **2003**, *125*, 4976−4978.
(22) Roggenbuck, J.; Tiemann, M. *J. Am. Chem. Soc.* **2005**, *127*, 1096−1097.
(23) Schwickardi, M.; Johann, T.; Schmidt, W.; Schüth, F. *Chem. Mater.* **2002**, *14*, 3913−3919.
(24) Li, W.-C.; Lu, A.-H.; Weidenthaler, C. M.; Schüth, F. *Chem. Mater.* **2004**, *16*, 5676−5681.
(25) Jun, S.; Joo, S. H.; Ryoo, R.; Kruk, M.; Jaroniec, M.; Liu, Z.; Ohsuna, T.; Terasaki, O. *J. Am. Chem. Soc.* **2000**, *122*, 10712−10713.

Table 1. Comparison of the d_{100} Values and Cell Constants *a* (Corresponding to the Hexagonal Pore Arrangement), the Average Pore Diameters, the Specific Surface Areas (Calculated by the BET Method), and the Pore Volumes in SBA-15 Silica, CMK-3 Carbon, and Mesoporous MgO[a]

	d_{100} (nm)	*a* (nm)	pore diam[b] (nm)	wall thickness (nm)	BET surface area (m^2g^{-1})	pore vol[b] (cm^3g^{-1})
SBA-15	9.9	11.4	10.2	1.2	520	1.26
CMK-3	8.8	10.2	4.0	6.2	830	0.67
MgO	8.7	10.1	7.0	3.1	280	0.52

[a] The wall thicknesses are calculated as the difference between cell constants and pore diameters. [b] From analysis based on NLDFT data.

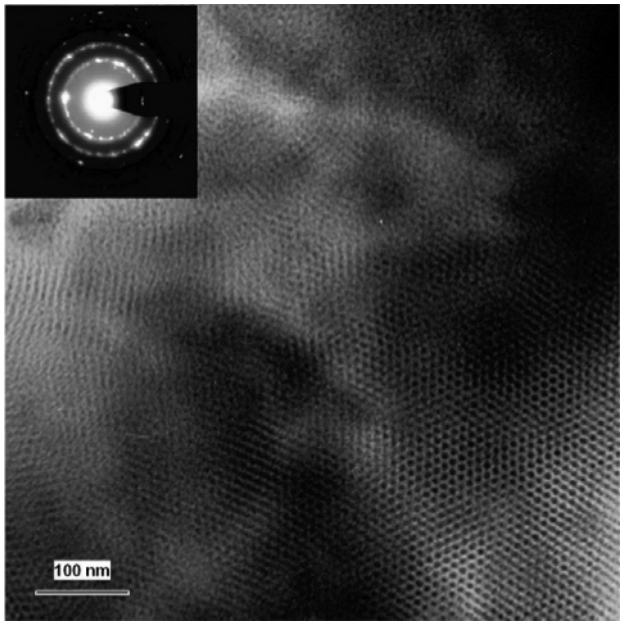

Figure 2. TEM image of mesoporous MgO showing long-range periodicity in the hexagonal pore arrangement. The SAED pattern confirms that the pore walls are crystalline.

stantial nonporous byproducts was found; EDX analysis confirms the absence of significant amounts of silica. The SAED pattern exhibits concentric diffraction rings with single, weakly resolved spots on top of them. This is indicative of rather small, though well-ordered, crystalline domains, the exact size of which cannot be determined in a straightforward way. Application of Scherrer's formula to the X-ray wide-angle diffractions suggests domain sizes between 6.5 and 7.5 nm, which are a little larger than the estimated pore wall thickness (see below). However, owing to the limited accuracy of Scherrer's formula, especially when the domain shape is ill-defined (which is the case here), these values should be regarded as rough estimates only.

Nitrogen physisorption isotherms of the samples from Figure 1 are shown in Figure 3. The isotherms for both SBA-15 silica and mesoporous MgO are of type IV and show H1 hysteresis; i.e., the adsorption and desorption branches are parallel,[26] as expected for regular, cylindrical mesopores. The specific surface areas (calculated by the BET method) are shown in Table 1. The lower surface area of the mesoporous MgO sample (280 m^2 g^{-1}) as compared to the original SBA-15 silica (520 m^2 g^{-1}) can partly be attributed to the fact that the densities of the two materials are different. In the bulk phase MgO has a density of 3.6 g cm^{-1}, while that of amorphous SiO_2 is approximately 2.2 g cm^{-1}.[27] It is reasonable to assume similar differences in the densities for the pore walls of the mesoporous samples; therefore, the surface areas of mesoporous MgO and SBA-15 silica are closer to each other when normalized with respect to the density. However, even with this normalization, the MgO sample still has a lower specific surface area, which can be accounted for by the above-mentioned partial loss of structural order during the two replication steps as well as by a lower relative degree of microporosity in the MgO sample as compared to SBA-15. The pore diameter distributions are displayed in Figure 4, and the average (i.e., distribution peak) values as well as the pore volumes are listed in Table 1. It is generally understood that for pores smaller than ca. 10 nm the BJH method (Figure 4, top) underestimates the pore diameters

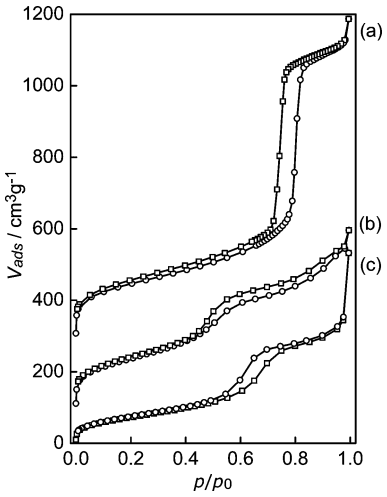

Figure 3. Nitrogen physisorption isotherms of (a) SBA-15 silica, (b) CMK-3 carbon, and (c) mesoporous MgO (circles, adsorption; squares, desorption). For clarity, curves a and b are vertically shifted in steps of 150 cm^3 g^{-1}.

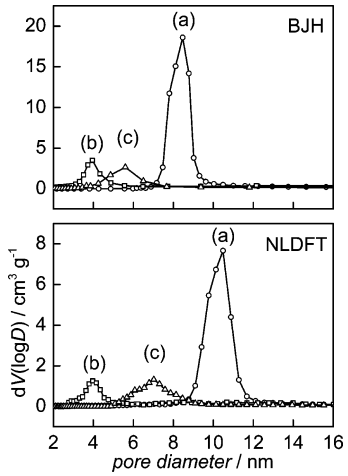

Figure 4. Pore size distributions of (a) SBA-15 silica, (b) CMK-3 carbon, and (c) mesoporous MgO, determined by the BJH method (top) and by analysis based on NLDFT data (bottom).

(26) Sing, K. S. W.; Everett, D. H.; Haul, R. A. W.; Moscou, L.; Pierotti, R. A.; Rouquérol, J.; Siemieniewska, T. *Pure Appl. Chem.* **1985**, *57*, 603−619.

(27) *Handbook of Chemistry and Physics*, 76th ed.; Lide, D. R., Ed.; CRC: Boca Raton, FL, 1995; pp 4−98.

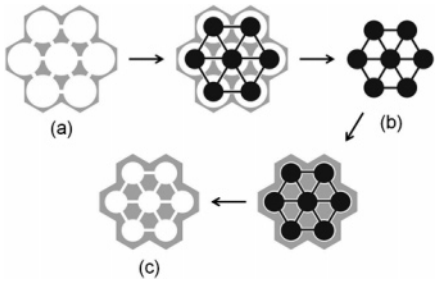

Figure 5. Simplified schematic representation (view along the pore axis) of the double replication process from (a) SBA-15 silica over (b) CMK-3 carbon to (c) mesoporous MgO. The scaling of the mesopore diameters and wall thicknesses corresponds to the analytical values in Table 1. This idealized picture is only supposed to deliver a visual impression on the relative proportions.

by up to 25%.[28] Pore size analysis based on data obtained from NLDFT calculations is therefore much more reliable (Figure 4, bottom). However, NLDFT-based analysis is only applicable if data kernels are available which correspond to the specific pore shape and to the physical/chemical nature of the pore surface. No specific kernel is presently available for MgO; instead, we have chosen the kernel for SiO_2 (cylindrical pores, N_2 sorption at 77 K), which delivers identical pore size distributions for the adsorption isotherm, using the spinodal condensation method, and for the desorption isotherm, using the equilibrium method. This agreement between the two methods confirms the regular cylindrical pore shape, i.e., the absence of network effects, such as pore blocking or percolation, consistent with the occurrence of H1 hysteresis;[28] it is also a strong indication that application of the SiO_2 data kernel to MgO (with cylindrical pores) is justified due to apparently sufficient similarity in the pore surface properties. For CMK-3 carbon we have used the kernel for slitlike pores, which may introduce some error, since the pores in CMK-3 carbon have a more complicated shape; however, we again obtain identical results from both isotherm branches, which may serve as an indication that it is legitimate to apply this kernel. It should also be noted that the inaccuracy of the BJH method is much less significant for mesoporous carbons than for materials with polar surface functions (such as SiO_2 and MgO); accordingly, the BJH- and NLDFT-derived pore diameter distributions are quite similar in this case. In summary, in all three samples (SBA-15, CMK-3, and MgO) we regard the average pore diameters obtained from the NLDFT-based analysis as much more reliable than those from the BJH method.

By subtracting the average pore diameters (obtained from the NLDFT-based analysis) from the cell constant a of the hexagonal pore arrangement (calculated from the X-ray diffraction patterns: $a = 2d_{100}/\sqrt{3}$), we obtain an estimation of the respective pore wall thicknesses; the results are shown in Table 1. Figure 5 depicts a schematic representation of the pore sizes and wall thicknesses according to these results; it needs to be stressed that this picture is strongly simplified and only designed to visualize the relative proportions listed in Table 1. We find that in the first replication step the pores in SBA-15 silica are not completely filled with carbon; this is consistent with the existing literature.[18] Contrary to that, the second replication step yields a much more efficient filling of the CMK-3 carbon pores with MgO. This may be attributable to a higher degree of pore interconnection in CMK-3 than in SBA-15, leading to a more efficient distribution of the MgO precursor species by diffusion.

(28) Thommes, M. In *Nanoporous Materials: Science and Engineering*; Lu, G. Q., Zhao, X. S., Eds.; Imperial College Press: London, 2004; pp 317−364.

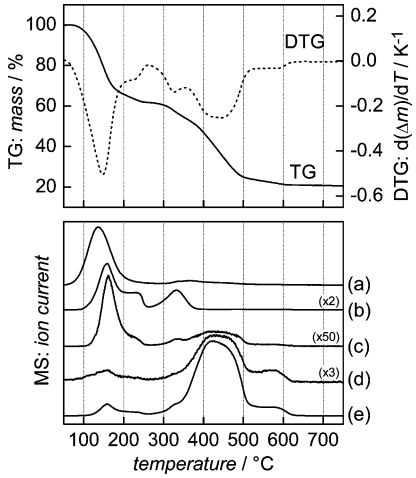

Figure 6. Coupled thermogravimetry and mass ion detection for mesoporous CMK-3 carbon impregnated with $Mg(NO_3)_2$. The mass loss (TG) occurs in several steps (visualized by the first derivative of the TG curve, DTG) and is accompanied by the detection of several mass fragments: (a) H_2O^+ ($m/z = 18$), (b) NO^+ (30), (c) NO_2^+ (46), (d) CO^+ (28), (e) CO_2^+ (44).

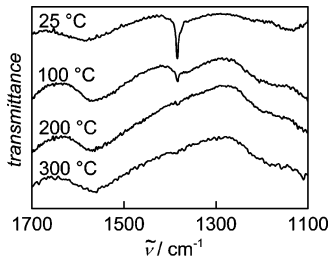

Figure 7. IR spectra of mesoporous carbon impregnated with $Mg(NO_3)_2$ after heating to various temperatures. The disappearance of the asymmetric stretching vibration of the nitrate anion at 1385 cm^{-1} shows that the conversion of $Mg(NO_3)_2$ to MgO takes place in a temperature range below ca. 200 °C.

To study the formation of MgO inside the porous carbon matrix, we have performed thermal analysis under flowing air on a CMK-3 sample impregnated with $Mg(NO_3)_2$; Figure 6 shows the coupled TG and mass ion detection. The TG curve shows a mass loss occurring in several steps, more clearly visible in the first derivative (DTG). However, the overall mass decrease can be roughly divided into two parts: In a first temperature interval between 50 and 270 °C the mass is reduced to approximately 62% of the initial value. This step is accompanied by the detection of mainly residual (presumably physisorbed) water ($m/z = 18$) and nitric oxides (NO, $m/z = 30$; NO_2, $m/z = 46$). The latter originate from the conversion of $Mg(NO_3)_2$ to MgO. This is confirmed by temperature-resolved ex situ IR spectroscopy (Figure 7), which probes the presence of the nitrate anion by its characteristic asymmetric stretching vibration at 1385 cm^{-1}; the band's intensity is reduced with increasing temperature and is no longer detectable above ca. 200 °C. Another step in the TG curve follows between 270 and 600 °C, after which

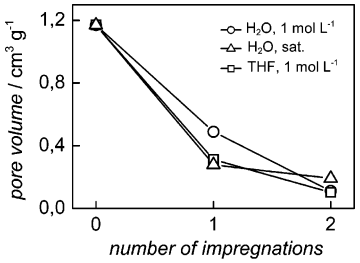

Figure 8. Pore volume of mesoporous CMK-3 carbon before and after (repeated) impregnation with $Mg(NO_3)_2$. Each impregnation cycle comprises filtration, drying, and conversion of $Mg(NO_3)_2$ to MgO as described in the Experimental Section. The reduction of the pore volume, i.e., the efficiency of the impregnation, is mostly independent of the choice of impregnation technique. For this study a CMK-3 carbon sample with large relative pore volume (1.17 $cm^3\ g^{-1}$) was chosen for high accuracy; the average pore diameter (3.6 nm) corresponds to that in the sample from Table 1, but the wall thickness is lower (4.8 nm).

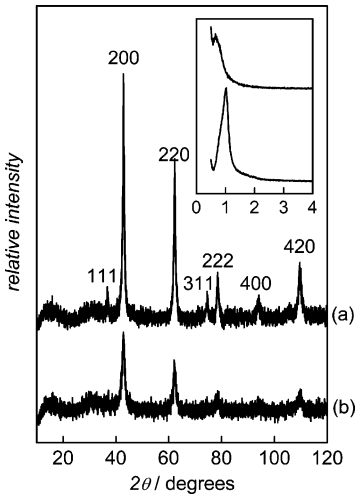

Figure 9. Powder X-ray diffraction diagrams of mesoporous MgO samples which were synthesized (a) with and (b) without tempering at 823 K in a vacuum before the removal of the carbon matrix. The tempered sample exhibits narrower reflections in the wide-angle region, indicating a higher degree of crystallinity; the shift of the low-angle reflections toward lower angle reveals a change in the mesostructural order.

the mass arrives at a constant value of ca. 21%. During this step carbon oxides (CO, $m/z = 28$; CO_2, $m/z = 44$) are generated, attributable to the thermal combustion of the porous carbon matrix. However, NO is still detected up to ca. 380 °C, indicating that the temperature range for the formation of MgO slightly overlaps with the oxidation of the carbon. (The very weak occurrence of the $m/z = 46$ mass fragment above 380 °C is attributable to CO_2 with the isotope composition $^{12}C^{16}O^{18}O$ rather than to NO_2.) These findings demonstrate that conversion of $Mg(NO_3)_2$ to MgO under air bears the risk of structural loss due to premature decomposition of the carbon matrix, especially when a second impregnation with $Mg(NO_3)_2$ is supposed to follow. The sample should therefore not be heated to a temperature higher than 270 °C.

The efficiency of the impregnation of the carbon matrix with $Mg(NO_3)_2$ needs to be maximized; i.e., the loading of the carbon pores should be as high as possible. We have varied the concentration of the $Mg(NO_3)_2$ solution from 1 mol L^{-1} ("wet impregnation") to saturation (ca. 3.8 mol L^{-1}, "incipient wetness"). To reach a higher wettability of the nonpolar carbon surface, we have also used THF as the

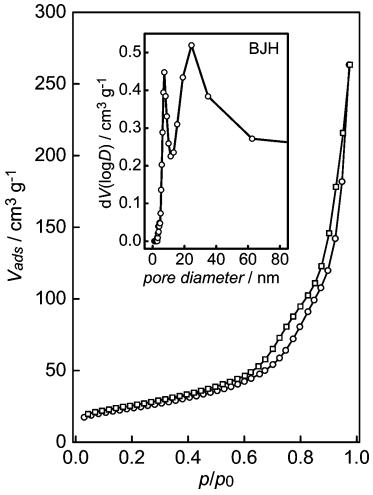

Figure 10. Nitrogen physisorption isotherm of mesoporous MgO which was tempered at 823 K in a vacuum before the removal of the carbon matrix (circles, adsorption; squares, desorption). The BJH pore size distribution (inset) reveals a much lower degree of regular porosity compared to that of a sample synthesized without tempering (see Figure 3).

solvent for $Mg(NO_3)_2$, although this reduces the solubility of the salt. However, it has turned out that these modifications of the impregnation process have only limited impact on the amount of $Mg(NO_3)_2$ that is deposited in the carbon pores. This is shown in Figure 8, where the decrease in pore volume in CMK-3 after one and two impregnation cycles is plotted for three different impregnation attempts. It is apparent that the degree of pore filling is comparable in all three cases, especially after the second cycle.

Apart from the impregnation technique we have explored other means of improving the synthesis of mesoporous MgO. In particular, the impact of various temperature programs for the formation of MgO as well as for the subsequent combustion of carbon was systematically studied. The optimum temperatures of 573 K for the conversion of $Mg(NO_3)_2$ to MgO and 1023 K for the carbon combustion were identified by thermal analysis (see above). Higher temperatures for the carbon combustion sometimes resulted in lower specific surface areas in the products. As expected, we found that lower combustion temperatures can be compensated for by longer duration; thus, the temperature was not allowed to exceed 1023 K and was kept constant for 2 h. The heating ramp of 2.5 K min^{-1} for both steps was found to be the most efficient. Raising the heating rate to 5 K min^{-1}, especially during the carbon combustion, resulted in increasing structural loss; faster heating led to complete destruction of the mesostructural order. Heating rates lower than 2.5 K min^{-1}, on the other hand, did not further improve the structural properties of the products. In addition, we have explored the impact of tempering the MgO/carbon samples before removal of the carbon. For this purpose we have heated the samples to various temperatures under vacuum (2 K min^{-1}) to promote thermal annealing and improve crystallinity. A significant narrowing of the wide-angle X-ray reflections is observed after tempering at 823 K for 6 h, indicating a higher crystallinity (Figure 9); application of Scherrer's formula suggests crystallite sizes between 10 and 11 nm. However, nitrogen physisorption after the removal of the carbon matrix reveals that this thermal treatment leads to a significant loss

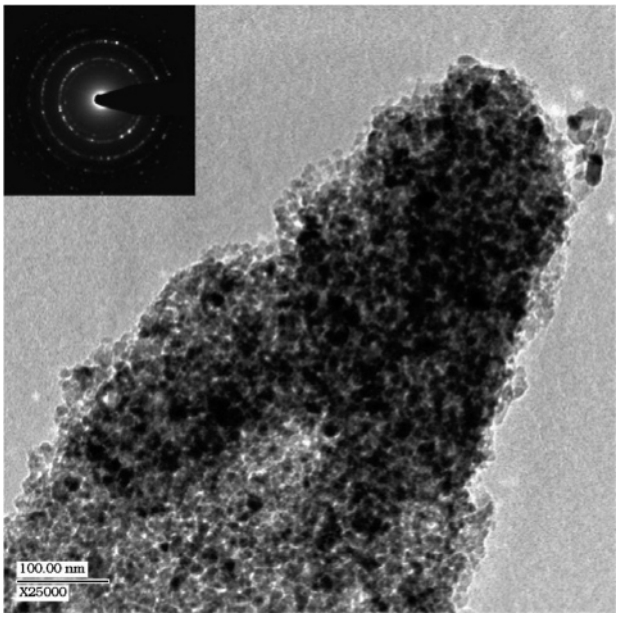

Figure 11. TEM image of mesoporous MgO which was tempered at 823 K in a vacuum before the removal of the carbon matrix. The sample exhibits large particles devoid of ordered mesopores. The SEAD pattern shows a higher crystallinity compared to that of a sample synthesized without tempering (see Figure 2).

in porosity; capillary condensation occurs at higher relative pressure, and the nitrogen uptake is altogether lower than in a sample which was not tempered (Figure 10). In the pore size distribution (calculated by the BJH method) the peak which corresponds to the ordered mesopores is broadened and is much weaker and slightly shifted from 6.6 to 7.4 nm (Figure 10, inset). The low-angle X-ray reflection is shifted toward lower angle, corresponding to a larger repeat distance (Figure 9, inset). An additional, very broad peak in the pore size distribution at ca. 25 nm is indicative of significant interparticle porosity. (Due to this ill-defined pore geometry the NLDFT-based pore size analysis is not practical here.) The specific surface area (BET) is decreased from 280 to 85 $m^2 g^{-1}$. TEM reveals that the tempered sample contains significant amounts of particles which lack regular intraparticle mesopores; the average size of these particles approximately corresponds to the results obtained from Scherrer's formula (Figure 11). In summary, the thermal treatment apparently induces partial destruction of the mesoporous carbon matrix, leading to an agglomerate of MgO particles without regular mesopores. However, due to the small size of the particles the specific surface area is still nonnegligible. Similar products have recently been obtained by utilization of carbon aerogels as structure matrixes.[24]

Conclusions

In summary, we have introduced the first synthesis of periodically ordered mesoporous magnesium oxide. Consecutive structure replication using mesoporous SBA-15 silica and CMK-3 carbon has turned out to be a versatile means of obtaining crystalline products with uniform and regular pore systems. Thorough pore size analysis and in situ investigation of the MgO formation inside the carbon pore system provide comprehensive insight into the replication procedure, identifying the ideal synthesis parameters. This may prove helpful in future syntheses using porous carbon materials as structure matrixes.

Acknowledgment. We thank Prof. Michael Fröba for continuous support, Marie-Luise Wolff and Peter Betz for valuable help in the laboratory, Dr. Jan Hanss (University of Augsburg, Germany) for carrying out the thermal analysis, and Dr. Matthias Thommes (Quantachrome Instruments) for helpful discussion of the porosity measurements.

CM060740S